BIOCHEMISTRY
including biophysical chemistry & molecular biology

Article

pubs.acs.org/biochemistry

The Miscoding Potential of 5-Hydroxycytosine Arises Due to Template Instability in the Replicative Polymerase Active Site

Karl E. Zahn, April Averill, Susan S. Wallace,* and Sylvie Doublié*

Department of Microbiology and Molecular Genetics, University of Vermont, Burlington, Vermont 05405, United States

Supporting Information

ABSTRACT: 5-Hydroxycytosine (5-OHC) is a stable oxidation product of cytosine associated with an increased frequency of C → T transition mutations. When this lesion escapes recognition by the base excision repair pathway and persists to serve as a templating base during DNA synthesis, replicative DNA polymerases often misincorporate dAMP at the primer terminus, which can lead to fixation of mutations and subsequent disease. To characterize the dynamics of DNA synthesis opposite 5-OHC, we initiated a comparison of unmodified dCMP to 5-OHC, 5-fluorocytosine (5-FC), and 5-methylcytosine (5-MEC) in which these bases act as templates in the active site of RB69 gp43, a high-fidelity DNA polymerase sharing homology with human replicative DNA polymerases. This study presents the first crystal structure of any DNA polymerase binding this physiologically important premutagenic DNA lesion, showing that while dGMP is stabilized by 5-OHC through normal Watson−Crick base pairing, incorporation of dAMP leads to unstacking and instability in the template. Furthermore, the electronegativity of the C5 substituent appears to be important in the miscoding potential of these cytosine-like templates. While dAMP is incorporated opposite 5-OHC ∼5 times more efficiently than opposite unmodified dCMP, an elevated level of incorporation is also observed opposite 5-FC but not 5-MEC. Taken together, these data imply that the nonuniform templating by 5-OHC is due to weakened stacking capabilities, which allows dAMP incorporation to proceed in a manner similar to that observed opposite abasic sites.

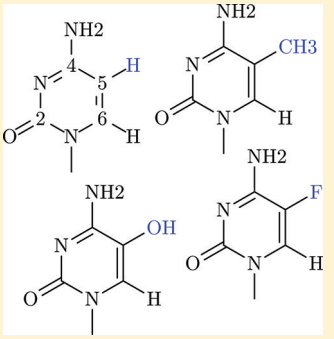

Evolution and disease are bound by an inextricable relationship that requires living creatures to balance the long-term benefits of low-level mutation against the deleterious effects of genomic instability. All life, including some viruses, is therefore obliged to resist unbridled mutation by conserving repair pathways capable of restoring covalently modified DNA. Aerobic organisms in particular must protect their genomes, not only from DNA-damaging ionizing radiation and toxic exogenous agents, but also from hydroxyl radicals generated as byproducts of metabolism.[1] Endogenous reactive oxygen species oxidize DNA bases and alter their base pairing specificity, which can lead to a mutation in the inevitable situation that an unrepaired base serves as a template for the replicative DNA polymerase.

Analysis of phylogenetic trees indicates that C → T transition mutations are abundant in the genomes of aerobic organisms.[2−4] Some of these mutations are due to the deamination of cytosine to uracil, which is kept in check by the uracil DNA glycosylase (UDG) and other related enzymes.[5−7] DNA glycosylases are key repair enzymes, given their responsibility to recognize and cleave the damaged base at the N-glycosylic bond prior to processing of the resulting abasic site through the base excision repair (BER) pathway, which concludes with insertion and ligation of a new nucleotide. Although mutation caused by cytosine deamination is easily understood due to dATP pairing with uracil during DNA synthesis, genetic manipulation of bacterial cells suggests that other oxidation products of cytosine also encode substantially for adenine. When the genes encoding Nth and Nei, two DNA glycosylases known to initiate repair of damaged pyrimidines, are knocked out in *Escherichia coli*, these cells experience a 43-fold increase in the rate of C → T transition.[8,9] 5-Hydroxycytosine (5-OHC) gained attention as a candidate premutagenic DNA lesion capable of increasing the frequency of C → T transitions when it was observed to pair with both dGMP and dAMP during in vitro DNA synthesis by the Klenow fragment (KF) of *E. coli* DNA polymerase.[10] Alternatively, 5-OHC was described as a potent premutagenic lesion causing C → T transitions by a method of reverse chemical mutagenesis, in which the mutational spectra of an uncharacterized oxidized cytosine analogue were analyzed in vivo and subsequently identified as 5-OHC.[11] When 5-OHC-containing DNA was transfected into wild-type bacterial cells, a modest increase in mutation frequency was observed, ∼10-fold above the measured background.[12]

5-OHC exists in DNA as a stable oxidation product. Oxidative addition at the C5−C6 double bond of cytosine yields the short-lived intermediate cytosine glycol, which then is dehydrated at the exocyclic C6 hydroxyl to 5-OHC. The potential for deamination at any point in this pathway, which is plausibly stimulated by oxidation of the C5−C6 bond,[13] relates 5-OHC to uracil glycol (UG) and 5-hydroxyuracil (5-OHU), two other premutagenic thymine-like bases. Because of the intact cytosine-like Watson−Crick (WC) face and normal minor groove functional groups of 5-OHC, however, it is not immediately clear how this particular oxidation product could pair with dAMP during replicative DNA synthesis. For this reason, we set out to elucidate a role for the C5

Received: August 4, 2011
Revised: September 30, 2011
Published: October 25, 2011

hydroxyl substituent in mismatch formation by the high-fidelity family B DNA polymerase from bacteriophage RB69 (gp43) by comparing DNA synthesis opposite templating dCMP, 5-methylcytosine (5-MEC), 5-OHC, and the nonphysiological base 5-fluorocytosine (5-FC). Through a combination of biochemical and structural approaches, we describe an enhanced efficiency for incorporation of dAMP opposite both 5-FC and 5-OHC but not 5-MEC by RB69 gp43. This study reveals the first crystal structures of any polymerase binding 5-OHC. Although guanine pairs stably with both 5-OHC and 5-FC by WC hydrogen bonding and is able to translocate to the postinsertion site of RB69 gp43, incorporation of dAMP at the primer terminus yields instability and disorder in the template. With dAMP, the DNA fails to translocate when 5-OHC or 5-FC is the templating base, and in both cases, the lesion tips away from the misincorporated dAMP, thus unstacking from the templating strand and creating a void resembling an abasic site. This particular conformation is reminiscent of a previously described ternary complex describing adenine mismatched with cytosine in the active site of DNA polymerase β (pol β).[14] Because favorable insertion of dAMP opposite abasic sites is a well-known phenomenon,[15−17] our observations imply that a similar mechanism explains the elevated efficiency of insertion dAMP opposite templating 5-OHC.

EXPERIMENTAL PROCEDURES

DNA, Reagents, and Proteins. Oligonucleotides were synthesized by Midland Certified Reagents (Midland, TX) and gel purified on a 16% polyacrylamide denaturing gel prior to use in crystallization and kinetic experiments. The 18-mer sequence 5′-cc**X**ggtatgacagccgcg, where **X** was either 5-OHC, 5-FC, 5-MEC, or dCMP, was annealed to the 14-mer primer 5′-gcggctgtcatacc, placing the modified base in templating position and leaving an unpaired dGMP at the 3′ end of the template strand to make important crystal contacts.[18] For the 5-OHC·dGMP structure, the 15-mer primer 5′-gcggctgtcataccg with dGMP synthesized at the 3′ terminus was used because ddGMP incorporated in the crystallization drop spoiled crystal growth. For the kinetic experiments, the 14-mer oligonucleotide primer was labeled with 5′-tetrachlorofluorescein (5′-TET) for visualization at 532 nm. Nucleoside triphosphates were purchased from Fisher Scientific (Pittsburgh, PA). Polyethylene glycol 2000 monomethyl ether (PEG 2000-MME) was from Hampton Research (Aliso Viejo, CA). All other salts and buffers were purchased from either Fisher Scientific or Sigma-Aldrich (St. Louis, MO). RB69 gp43 exo- (D222A, D327A) was expressed in *E. coli* BL21(DE3) cells and purified by merit of a C-terminal three-His tag as described previously.[19]

Pre-Steady-State Enzyme Kinetics. Reaction conditions for the evaluation of k_{pol} and K_D were identical to those published elsewhere.[20] Briefly, a 4-fold molar excess of RB69 gp43 exo- (2000 nM) was preincubated with 500 nM primer·template in 25 mM Tris acetate (pH 7.5), 50 mM sodium chloride, 1 mM β-mercaptoethanol (β-ME), and 0.5 mM EDTA, prior to addition of 20 mM magnesium acetate and the incoming nucleotide. Reactions evaluating pre-steady-state incorporation of dAMP (10−2000 μM) were slow enough to be undertaken by manual quenching with 100% formamide on the benchtop over a time course of 6−600 s. Reaction profiles of incorporation of dGMP (1−500 μM) opposite 5-OHC and dCMP required use of a RQF-3 rapid quench apparatus (KinTek, Austin, TX), because of the brisk experimental time course of 0.003−10 s, and were quenched with 0.5 M EDTA (pH 8.0). All reaction mixtures were run through a 16% polyacrylamide gel to separate extended from unextended primers, analyzed at 532 nm on a Bio-Rad (Hercules, CA) molecular imager FX by excitement of the 5′ TET, and quantified with Quantity-One (Bio-Rad). Except for reactions placing dGMP opposite 5-OHC, data were fit to the single-exponential curve $y = A(1 - e^{-k_{obs}t}) + C$, where y is the fraction extension, to yield k_{obs} for six nucleotide concentrations. Under identical conditions, a reduced pre-steady-state burst amplitude was observed for the 5-OHC template with incoming dGTP, and these reactions were therefore fit to the burst equation $y = A(1 - e^{-k_{obs}t}) + k_{ss}t$, where k_{ss} is the rate of the subsequent linear phase. The k_{obs} values derived from both methods were then used to fit the equation $k_{obs} = k_{pol}[dNTP]/(K_D + [dNTP])$. GNUplot was used for curve plotting and fitting.

Crystallization and Cryoprotection. RB69 gp43 exo- (100 μM) was cocrystallized in complex with 120 μM duplex DNA by hanging drop diffusion over 1 mL reservoirs containing 100 mM sodium acetate, 100 mM magnesium sulfate, 100 mM Hepes (pH 6.6−7.0), 5% glycerol (v/v), and 1 mM β-ME with 7−12% (v/v) PEG 2000-MME serving as the precipitant.[17] For the 5-OHC·dA and 5-FC·dA complexes, 2.3 mM dATP was added to the crystallization reaction mixture for enzymatic incorporation opposite the modified template. The 5-FC·ddG reaction mix contained only 1 mM ddGTP, whereas the 5-OHC·dG complex required no nucleotide because dGMP was added synthetically to the 3′-end of the primer, which was annealed to the 5-OHC template. Rectangular crystals ranged in size from 100 μm × 60 μm × 60 μm for the 5-FC·dAMP complex to 200 μm × 80 μm × 80 μm for the 5-OHC·dAMP complex, while the guanine complexes were of intermediate size. Crystals were cryocooled via addition of 2−3 μL of a solution of 50% glycerol (v/v) and 10% PEG 2000-MME directly to the hanging drop before the crystal was scooped and plunged into liquid nitrogen.

Data Collection. Beamlines ID23-B and ID23-D at the Advanced Photon Source (APS) were utilized for collection of X-ray diffraction data on a MAR Research (Norderstedt, Germany) m300 CCD detector under cryocooled conditions (100 K). Intensities were integrated and scaled with the Denzo/Scalepack.[21] Data from multiple crystals were merged when available (Table 2), yielding a high redundancy of reflection observations.[22]

Refinement of Structures. All four crystal structures belonged to primitive monoclinic space group $P2_1$ with four protein·DNA complexes per asymmetric unit (termed A−D), as expected for binary complexes of RB69 gp43 exo- crystallized under these conditions.[16,20,23] The refinement began with rigid body fitting of protein domains by CNS 1.2,[24] using as a starting model a binary complex of RB69 gp43 exo- [Protein Data Bank (PDB) entry 2P5G[17]] after omission of the DNA to avoid introducing model bias into the new structure. The starting model placed the fingers and thumb domains of all protein molecules in a conformation consistent with previous observation of open binary complexes of gp43. Following minimal rebuilding, helical density was apparent in the DNA binding cleft and polymerase active site of RB69 gp43, ruling out the possibility of an editing complex, which has been observed previously with molecules B and D when an abasic site resides in the templating position.[16] Iterative rebuilding with Coot[25] and refinement with Refmac 5.6[26] were conducted until the last step, when the modified templating bases were added to the DNA models. All protein residues mapped to the allowed region of the Ramachandran plot except Thr622, which

Table 1. Pre-Steady-State Kinetics for Incorporation of dAMP opposite Cytosine-like Templates[a]

template	incoming nucleotide	k_{pol} (s^{-1})	K_d (μM)	k_{pol}/K_d ($s^{-1}\ \mu M^{-1}$)	enhancement above A·C mismatch
dCMP	dATP	0.082 (0.0018)	1600 (280)	5.3 (0.91) × 10^{-5}	1.00
5-MEC	dATP	0.10 (0.020)	2200 (290)	4.6 (0.44) × 10^{-5}	0.87
5-FC	dATP	0.16 (0.011)	1300 (190)	13 (1.8) × 10^{-5}	2.4
5-OHC	dATP	0.27 (0.089)	960 (250)	27 (3.6) × 10^{-5}	5.2
furan[b]	dATP	0.36 (0.02)	1900 (240)	19 × 10^{-5}	3.6
dCMP	dGTP	89	14	6.6	1.2 × 10^5
5-OHC	dGTP	100	15	7.0	1.3 × 10^5

[a]Error estimates in parentheses represent the standard deviation on three replicate experiments. The enhancement above an A·C mismatch was calculated by dividing the catalytic efficiencies (k_{pol}/K_d) for each experiment by that calculated for the A·C mismatch. [b]The indicated values for furan opposite dATP were from ref 38.

is a conserved palm residue near the catalytic aspartates and is always noted as an outlier.[17,18] Because TLS parameters describing movement of individual protein domains were utilized for the Refmac refinement, the *B* factors reported in Table 1 were calculated with TLSANU.[27] Of the four protein·DNA complexes in all structures, protein chain C complexed to DNA chains I and J produced the best model when dAMP was incorporated at the primer terminus. For the (d)dGMP structures, protein chain B and DNA chains G and H demonstrated the least disorder. Our discussion therefore focuses on chains C, I, and J for the dAMP complexes and chains B, G, and H for the guanine complexes. All illustrations of these structures were generated with the Pymol Molecular Graphics System (Schrödinger, LLC, New York, NY).

RESULTS

Exonuclease-Deficient RB69 gp43 Incorporates dAMP opposite 5-OHC Templates. The incorporation specificity of DNA polymerases varies for the same DNA lesion depending on certain properties of the polymerase active site. Prior to this study, the only in vitro assays investigating the incorporation specificity of 5-OHC utilized KF,[10] a high-fidelity family A DNA polymerase, polymerase ι (pol ι), a low-fidelity specialized polymerase of the Y family, and the repair polymerase pol β.[28] To make this work relevant to replicative human DNA synthesis and disease, we employed the high-fidelity family B DNA polymerase from bacteriophage RB69.[18,29,30] This enzyme shares substantial homology with human polymerases δ and ε, which catalyze the majority of DNA synthesis in dividing human cells.[31]

Family B DNA polymerases often encode an accessory 3′−5′ exonuclease proofreading domain, which increases the fidelity of replication by ∼2 orders of magnitude.[32] Because this domain is tenacious for degrading DNA in vitro (Figure S1 of the Supporting Information), the incorporation specificity opposite 5-OHC was evaluated with an exonuclease-deficient (exo-) variant of RB69 gp43 in which two catalytic aspartates are mutated to alanines (D222A/D327A). Interestingly, the nucleotides selected for insertion opposite 5-OHC were similar to those inserted opposite 5-MEC, 5-FC, and an unmodified dCMP template, suggesting that the mutagenic potential of 5-OHC is due to small differences in the dynamics of incorporation (Figure 1). All the templates investigated served efficiently for error-free insertion of dGMP. To a lesser extent, dAMP was incorporated opposite each analogue, with a slight qualitative preference for the 5-FC and 5-OHC templates (Figure 1, lanes 12 and 17). Although C → A transversions are not common biological mutations, RB69 gp43 exo- incorporated dTMP opposite 5-OHC, 5-FC, and dCMP,

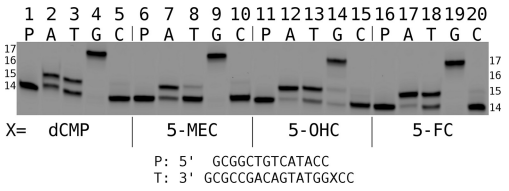

Figure 1. RB69 gp43 exo- (2 μM) incorporates 10 μM dGMP ≫ dAMP > dTMP and no dCMP opposite each 5-substituted cytosine-like template (0.5 μM) after 5 min. The 14-mer primer is extended by three bases to a 17-mer in the dGTP reaction because of the sequence context of the template oligonucleotide.

with 5-MEC being largely resistant to this mispairing. None of the DNA template bases directed substantial incorporation of dCMP.

The Level of Misincorporation of dAMP Is Elevated opposite 5-OHC and 5-FC. To quantify the relative efficiency of misincorporation opposite the substituted cytosine templates, we evaluated pre-steady-state kinetics to obtain K_d and k_{pol} values for dAMP (Table 1). As anticipated, curves describing incorporation of dAMP opposite 5-MEC and dCMP were largely identical, showing that a nonpolar hydrophobic moiety adjacent to C5 in the major groove does not impact nucleotide incorporation. On the other hand, the catalytic efficiency for incorporating dAMP opposite 5-FC and 5-OHC was enhanced 2.4- and 5.2-fold, respectively, over the normal biological bases. These observations imply that the electronegativity of the 5-hydroxyl and 5-fluoro substituents contributes to the formation of C·A mismatches, although the superior enhancement of the 5-OHC template suggests that electronegativity might provide only a partial explanation.

5-OHC Pairs with dGMP via Normal Watson−Crick Base Pairing. A binary complex of RB69 gp43 exo- was cocrystallized with a primer·template containing dGMP at the primer 3′-end such that this terminal base paired with 5-OHC in the template strand. Although efforts to cocrystallize RB69 gp43 by enzymatic incorporation of ddGTP into the template·primer failed, this alternate technique produced diffraction quality crystals allowing a well-ordered base pair between 5-OHC and dGMP to be visualized at 2.8 Å resolution (Table 2), revealing how the unmodified WC face of 5-OHC hydrogen bonds with dGMP in a typical fashion (Figure 2). Furthermore, because 5-OHC does not perturb the minor groove of the DNA double helix, the 5-OHC·dGMP base pair was able to translocate from the insertion site (n) to the postinsertion site ($n - 1$) and engage in water-mediated interactions with Tyr567 and Thr622, two conserved residues known to interact with the minor groove side of bases at the $n - 1$ site in this manner.[16,18]

Table 2. Data Collection and Refinement Statistics

	5-OHC·dGMP	5-OHC·dATP	5-FC·ddGMP	5-FC·dAMP
PDB entry	3TAB	3TAE	3TAF	3TAG
		Data Collection		
space group	$P2_1$	$P2_1$	$P2_1$	$P2_1$
cell dimensions				
a, *b*, *c* (Å)	132.8, 121.9, 168.9	133.3, 123.7, 165.9	133.0, 123.2, 169.3	132.8, 123.0, 165.2
α, *β*, *γ*, (deg)	90.0, 96.6, 90.0	90.0, 96.0, 90.0	90.0, 97.0, 90.0	90.0, 96.4, 90.0
resolution (Å)	30−2.80 (2.90−2.80)[a]	30−2.70 (2.80−2.70)[a]	30−3.00 (3.11−3.00)[a]	50−2.90 (3.00−2.90)[a]
no. of crystals	2	6	1	4
R_{merge} (%)[b]	17.6 (97.4)[a]	18.7 (91.0)[a]	8.4 (75.5)[a]	17.6 (100)[a]
$R_{Friedel}$ (%)[c]	9.0 (81.4)[a]	6.0 (52.0)[a]	9.4 (81.4)[a]	8.7 (67.9)[a]
$I/\sigma I$	8.3 (2.1)[a]	13.8 (3.0)[a]	14.8 (2.0)[a]	10.5 (2.2)[a]
no. of reflections	881770 (131768)[d]	2495386 (142643)[d]	428261 (107477)[d]	1119612 (117041)[d]
completeness (%)	99.9 (99.8)[a]	100 (100)[a]	98.9 (98.3)[a]	99.9 (100)[a]
redundancy	6.8 (5.2)[a]	17.5 (9.4)[a]	4.0 (3.9)[a]	9.6 (8.0)[a]
		Refinement		
resolution (Å)	30−2.80	30−2.71	30−3.0	30−2.95
no. of reflections	119040	128809	97064	100426
R_{work}/R_{free} (%)	23.2/28.1	22.4/26.8	23.3/28.0	23.9/28.4
root-mean-square deviation				
bond lengths (Å)	0.005	0.005	0.005	0.005
bond angles (deg)	0.870	0.925	0.840	0.839
B factor (Å^2)[e]				
protein chain				
A	93.5	65.5	86.9	67.9
B	75.1	105	73.6	114
C	77.6	70.3	70.2	71.7
D	123	143	118	135
DNA chain (template·primer)				
E/F	96.7/113	91.9/91.8	97.2/114	99.1/94.5
G/H	53.6/58.5	110/118	51.9/56.6	101/114
I/J	62.0/70.9	55.3/61.2	61.6/70.7	57.9/63.1
K/L	123/140	153/168	115/135	163/187
water	50.4	50.2	46.8	49.7

[a]Highest-resolution data are shown in parentheses. [b]$R_{merge} = \sum|I_{hkl,i} - \langle I_{hkl}\rangle|/\sum|I_{hkl,i}|$. [c]$R_{Friedel} = \sum|I_+ - \langle I_-\rangle|/\sum\langle I\rangle$. [d]The total number of reflections is shown. The number of unique observations is shown in parentheses. [e]Total *B* factors reported were derived from residual isotropic *B* factors with TLSANL,[27] following TLS refinement. The TLS refinement model contained protein residues only.

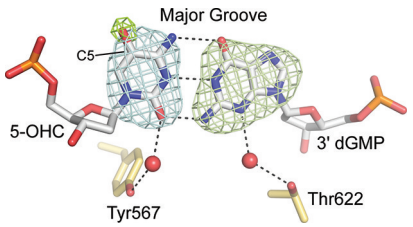

Figure 2. Close-up of the 5-OHC·dGMP base pair. Simulated annealing omit maps ($F_o - F_c$) are shown for dGMP (olive green, 3.3σ), 5-OHC (blue-green, 3.3σ), and the C5 hydroxyl group (bright green, 3.0σ). Hydrogen bonds shown as dashed lines are consistent with WC base pairing between 5-OHC and 3′-dGMP. The C5 hydroxyl does not preclude translocation of this base pair, which was resolved in the post-translocation ($n - 1$) site where conserved protein residues (Tyr567 and Thr622) make water-mediated interactions with the minor groove of the base pair.

The 5-OHC Template Becomes Disordered When dAMP Is Incorporated at the Primer Terminus. Enzymatic incorporation in the crystallization drop provided an effective strategy for trapping dAMP opposite 5-OHC in the active site of RB69 gp43 exo-. This technique produced larger crystals of higher quality compared to those with dGMP, which allowed the mismatch to be observed at a resolution of 2.7 Å. Interestingly, the configuration of the 5-OHC template did not suggest that a discrete hydrogen bonding pattern is required for incorporation of dAMP. Rather, the templating 5-OHC tipped away from the incorporated dAMP, creating a void reminiscent of an abasic site and negating the potential for any contacts with dAMP (Figure 3).[14] Although the dAMP stacked intrahelically under the primer strand and was built into electron density similar in quality to that of well-ordered double-stranded portions of the DNA, the templating 5-OHC exhibited higher *B* factors, suggesting that the template base experienced more relative disorder than the primer terminus base. The only potential for contacts between 5-OHC and protein residues appeared to be fortuitous and was observed at Lys279, a residue of the exonuclease domain that is not absolutely conserved. This residue has been observed previously contacting guanidinohydantoin, a lesion formed by oxidation of guanine, although mutating this lesion to alanine had no effect on lesion bypass or incorporation specificity.[33]

dx.doi.org/10.1021/bi201219s|*Biochemistry* 2011, 50, 10350−10358

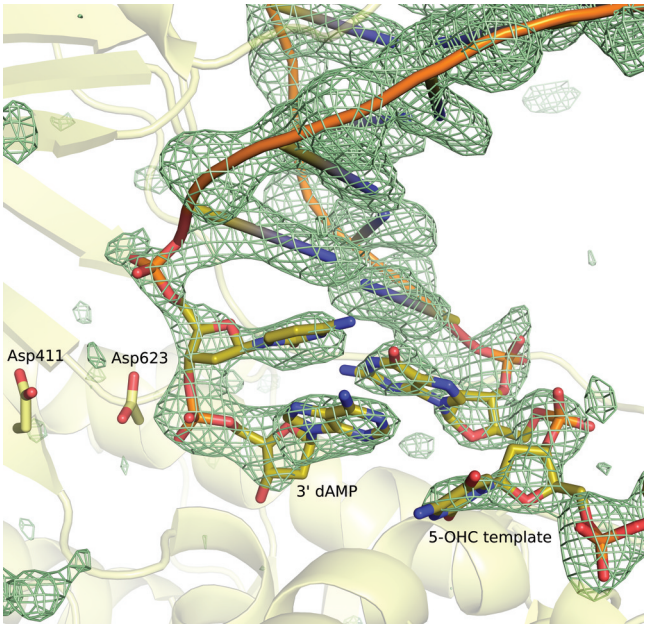

Figure 3. Close-up of the 5-OHC·dAMP complex. A simulated annealing omit map (green mesh, 3σ) shows residual density for the primer·template pair when dAMP is incorporated opposite 5-OHC. The lesion tips in the 5′-direction of the template, creating an abasic void in which the dAMP rests. The proximity of the metal chelating residues (Asp411 and Asp623) to the primer terminus indicates that this base pair failed to translocate and is stalled in the polymerase active site.

5-FC Reiterates the Observations of 5-OHC in the Active Site of RB69 gp43. To address the discrepancy between the kinetic efficiency of incorporation of dAMP opposite 5-FC versus 5-OHC, crystal structures of the 5-FC template opposite dAMP and ddGMP were also determined. This endeavor recapitulated the observations made with 5-OHC, showing that the 5-FC·ddGMP complex forms a translocated WC base pair, whereas the 5-FC·dAMP complex stalls with the templating base tipped away from the primer terminus (Figure 4). Analyzing the conformations of the DNA in terms of local interbase tilt, roll, and twist angles confirms the similarity of the lesions and primer termini in these structures, showing that both the mismatched 5-OHC and 5-FC are tipped approximately 60° relative to the adjacent base (Table S1 of the Supporting Information).[34] The mismatch appears to also induce disorder in the $n - 1$ base pair, which is demonstrated by reduced twist angles compared to the local interbase pair relationships exemplified by canonical DNA (Table S1 of the Supporting Information). Interestingly, the translocated conformation of the (d)dGMP structures does not appear to be a consequence of the crystallization method, because although dGMP was synthesized at the oligonucleotide primer terminus used in the 5-OHC structure, ddGMP was enzymatically incorporated by gp43 opposite 5-FC. The R factors comparing the intensity of equivalent reflections from isomorphous data sets (R_{cross}) also support the similarity between the 5-OHC and 5-FC complexes related by the incoming nucleotide and were calculated to be near 23% on intensities (I) in both cases. This high degree of isomorphism is presumably a consequence of the DNA translocation state. Comparing translocated (incoming guanine) to untranslocated (incoming adenine) complexes yields R_{cross} values on I in excess of 55%.

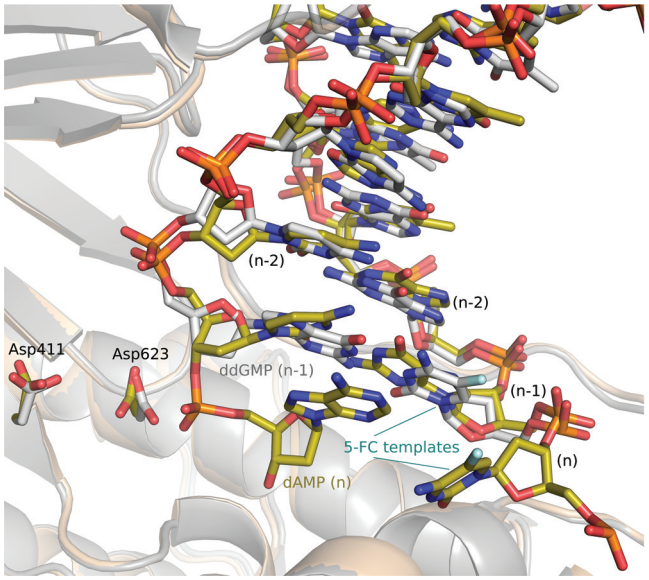

Figure 4. Superposition of the 5-FC·ddGMP and 5-FC·dAMP complexes. The 5-FC structures with ddGMP (gray carbon atoms) and dAMP (yellow carbon atoms) opposite the modified template are superimposed. The catalytic aspartates (Asp411 and Asp623) mark the insertion site. This view compares the translocation state of the ddGMP complex to that of the stalled dAMP structure. As with 5-OHC, the untranslocated modified template tips in the 5′-direction when paired with dAMP but translocates when opposite guanine (ddGMP here).

The Burst Phase for Incorporation of dGMP opposite 5-OHC Does Not Go to Completion. Although the structural comparison outlined similarities between 5-OHC and 5-FC templates, dissimilarities were evident in the primer extension assays monitoring dGMP incorporation, which routinely failed to reach completion for the 5-OHC template. Incorporation of 100 μM dGTP opposite all the templates progressed approximately 3 orders of magnitude faster than that with dATP, despite the singularly reduced pre-steady-state burst amplitude for the 5-OHC reaction (Figure 5 and Table 3). The reactions inserting dATP, although slow, ran to completion with the identical primer·template pairs, including those containing 5-OHC (Figure 5, inset).

To estimate the values of k_{pol} and K_d for dGTP opposite 5-OHC, the burst equation was utilized for calculation of k_{obs} over a range of dGTP concentrations. As anticipated for a substituent in the major groove of a modified DNA base, the C5 hydroxyl appeared to have little impact on the efficiency of dGMP incorporation where the enzyme was able to proceed forward with the reaction. Accordingly, the kinetic parameters compare favorably with those calculated here and elsewhere for formation of a dCMP·dGMP base pair (Table 1).[35] The presence of 5-OHC in the template strand appears to adjust the conformational equilibrium of RB69 gp43 toward the exonuclease complex, however, which produces a substantial population of stalled complexes potentially responsible for the reduced burst amplitude when the exo- variant is used. Accumulation of these exonuclease complexes is supported by comparison of the ability of RB69 gp43 exo- and wild-type enzymes in their ability to bypass 5-OHC and dA·dC mismatches. With exonuclease activity intact, wild-type RB69 gp43 shows a greater propensity to degrade primers annealed to 5-OHC containing templates than those with the unmodified template (Figure S1 of the Supporting Information).

dx.doi.org/10.1021/bi201219s|*Biochemistry* 2011, 50, 10350–10358

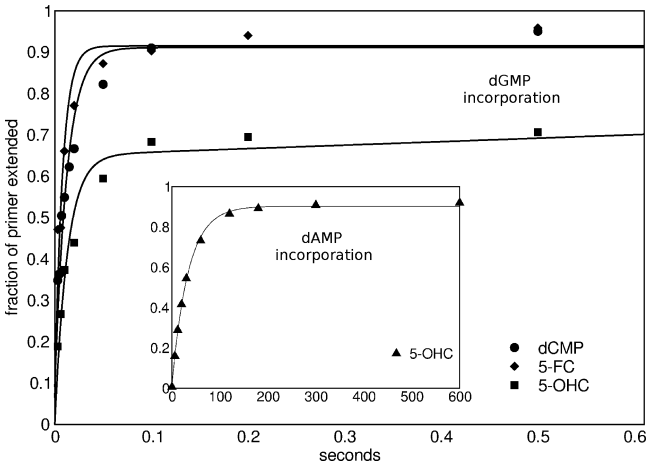

Figure 5. dGTP (100 μM) is incorporated by RB69 gp43 exo- (2 μM) opposite 5-OHC (■) rapidly, but with a burst amplitude extending only 0.65 of the primer·template (0.5 μM). The best fit graph was obtained by fitting the burst equation. Under identical reaction conditions, 5-FC (◆) and an unmodified dCMP template (●) do not show this reaction profile and rather allow full extension of the labeled primer. The primer·template containing 5-OHC is extended to completion with 100 μM dATP over a longer time course (▲, inset). Except for the assay pairing dGMP with 5-OHC, all primer extension profiles were fit to the pre-steady-state first-order exponential curve. Reaction constants describing these curves are listed in Table 3.

Table 3. Constants for the Primer Extension Assay Depicted in Figure 5[a]

template	incoming nucleotide	k_{obs} (s^{-1})	k_{ss} (s^{-1})	amplitude
dCMP	dGTP	79	N/A[b]	0.82
5-FC	dGTP	126	N/A[b]	0.85
5-OHC	dGTP	77	0.084	0.65
5-OHC	dATP	0.025	N/A[b]	0.87

[a]When dAMP is inserted opposite 5-OHC, the rate is decreased. When dGMP is inserted opposite 5-OHC, the amplitude is decreased. Except for the value for 5-OHC·dGTP, which was fit to the burst equation, all numbers represent values fitted to the first-order exponential. [b]Not applicable.

DISCUSSION

The crystal structures of RB69 gp43 bound to DNA containing 5-OHC provide the first description of this lesion in the active site of a DNA polymerase. In the 5-OHC·dAMP complex, the lesion tips away from the incorporated dAMP and adopts a configuration that suggests that 5-OHC may not hydrogen bond with dATP during alignment of the primer terminus for nucleophilic attack on the incoming nucleotide (Figure 3). The catalytic step captured in the crystal structure depicts the complex after covalent incorporation of dAMP, following reopening of the fingers domain from the closed, catalytically competent conformation. Although we cannot rule out the possibility that a different configuration of 5-OHC could drive selection of dATP earlier in the catalytic cycle, the newly refined model implies that such a base pairing would be transient if it exists, because no interactions between 5-OHC and dAMP are observed at this subsequent reaction step trapped in the crystal form. Because dAMP is known to be inserted opposite abasic sites, in particular because of the base stacking capabilities of adenine, the lack of contacts between dAMP and 5-OHC in the new crystal structure is consistent with base stacking playing a paramount role in nucleotide selection opposite this lesion.[16,17,36,37] Previous data from our laboratory examining insertion of dAMP opposite tetrahydrofuran, a stable abasic site analogue, show that RB69 gp43 exo- inserts dAMP opposite 5-OHC and abasic sites at comparable rates (Table 1), also consistent with the potential for similarity in the reaction mechanisms.[38]

The electron withdrawing ability of the extraneous hydroxyl moiety appears to be important in allowing dAMP to pair with 5-OHC. Although at a value somewhat lower than the catalytic efficiency (k_{pol}/K_D) of incorporation of dAMP opposite 5-OHC, dAMP is also incorporated opposite 5-FC with elevated facility over 5-MEC, the steric control. Because the crystal structures revealed no interactions between dAMP and the C5-substituted template bases, it appears unlikely that the electronegative moieties stabilize a preferable tautomer of the template able to encode dAMP by hydrogen bonding.[39,40] One alternative explanation might address the potential for reduced base stacking capabilities in 5-FC and 5-OHC templates. Pyrimidines are known to stack in DNA more weakly than purines, and it is possible that a fluorine or oxygen atom poised to withdraw electrons from the pyrimidine ring could exacerbate this trend and further compromise the ability of the base to stack properly as a template, thus increasing the probability for misincorporation of dAMP opposite the void introduced by the unstacked template. The human thymine DNA glycosylase (TDG) provides another example in which 5-OHC and 5-FC behave analogously in an enzyme's active site, which preferably cleaves both 5-OHC and 5-FC when paired opposite dGMP because the electronegative moieties allow the modified bases to serve as better leaving groups than normal cytosine during the cleavage reaction.[41]

Each primer·template pair interrogated by this study also readily directs incorporation of dGMP by RB69 gp43. However, the 5-OHC reaction appeared to be unique in that the amplitude of the burst phase was reduced compared to those with 5-FC, 5-MEC, and dCMP. Although the analogous reaction with dAMP was comparatively slow, the primer was extended to near completion without indication of a linear phase. Interestingly, we are not the first to observe depressed activity of a polymerase for insertion of dGMP opposite 5-OHC. Compared to dCMP, pol ι also demonstrated reduced standing-start activity on a primer·template pair containing 5-OHC under steady-state conditions.[28] Although RB69 gp43 exo- appears to bind some fraction of the 5-OHC-containing primer·template molecules in the nonproductive exonuclease mode (Figure S1 of the Supporting Information), this explanation does not apply to pol ι, which possesses only a single catalytic mode.

The incorporation specificity by RB69 gp43 exo- with an undamaged templating dCMP closely resembles that of 5-OHC in our standing-start primer extension assays (Figure 1). The qualitative similarity of these experiments could indicate that mismatches form by identical mechanisms opposite all the templates investigated, in which chemical properties of the base, such as a reduced level of template base stacking because of the electronegativity of the C5 substituent, adjust the relative efficiency of incorporation in favor of error-free or error-prone DNA synthesis. Given these biochemical parallels, the overwhelming similarities of the 5-OHC and 5-FC complexes further encourage interpretation of the new crystal structures with reference to previously reported dCMP·dA mismatch structures in which the templating base is unmodified.

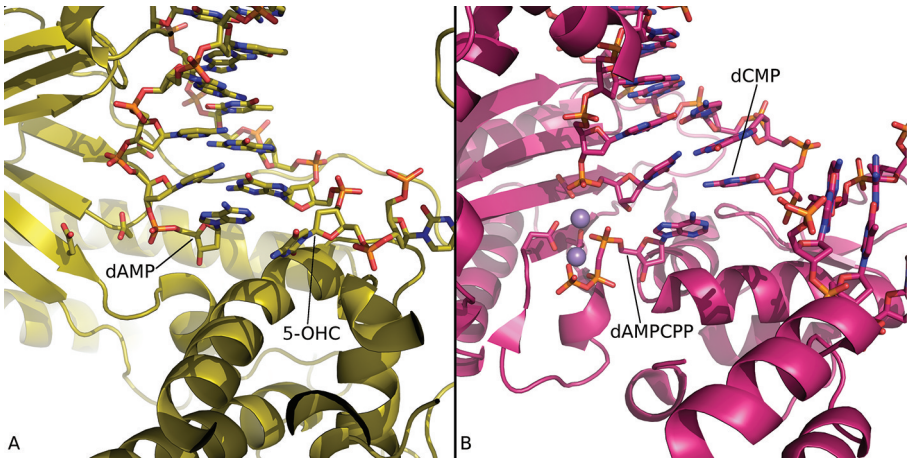

Figure 6. RB69 gp43 inserts dAMP opposite 5-OHC in a manner comparable to that by which polymerase β coordinates a dATP analogue opposite templating dCMP. (A) 5-OHC·dAMP structure (PDB entry 3TAE) in which the lesion has unstacked and tipped away from base pair $n - 1$. (B) Analogous view of polymerase β (PDB entry 3C2L[14]), which orients the incoming dAMPCPP opposite dCMP such that the template likewise provides no contact with the incoming adenine base.

Dodecanucleotides designed with an intrahelical A·C mismatch have been examined previously by both NMR and X-ray crystallography, revealing that a wobble base pair often stabilizes the mismatch in double-stranded DNA.[42,43] The active sites of DNA polymerases, however, provide a unique DNA environment, which would be difficult to approximate outside of the enzyme. Of particular interest is the orientation of the upstream single-stranded template DNA, which generally takes a sharp turn away from the active site in most DNA polymerases and is stabilized in its extrahelical orientation by aromatic or basic protein residues (e.g., Trp574 in RB69 gp43). Therefore, in B family polymerases, the templating base has no stacking partner in the 5′-upstream direction, which creates the space in which we observed 5-OHC and 5-FC when paired with dAMP. The fragment of *Bacillus* Pol I (BF), though a very useful crystallographic tool for describing formation and extension of several other mismatches, did not stabilize A·C or C·A mismatches when such complexes were crystallized.[44] On the other hand, crystallization of polymerase β binding DNA and dAMPCPP, a nonhydrolyzable dATP analogue, produced a ternary complex describing adenine opposite a cytosine template.[14] Interestingly, like our binary complexes of dAMP opposite 5-OHC, this structure also revealed no contacts between the incoming dATP analogue and the template (Figure 6). The fact that the polymerase β mismatched ternary complex depicts the fully assembled replication complex, with nucleoside triphosphate and divalent metal ions bound in the active site, is of substantial interest in light of the new postincorporation complexes from this study, because together these structures demonstrate the potential for a transient abasic site at steps of the polymerase catalytic cycle both prior to and sometime after nucleophilic attack.[14]

CONCLUSIONS

Certain mutations occur with greater frequency over time, presumably because of differential biological outcomes associated with specific DNA damage. In particular, the predominance of C → T transitions observed in aerobic organisms has been a conundrum, because it remains unclear which lesions are predominantly responsible for this well-established observation. Deamination of cytosine to uracil, or 5-OHC to 5-OHU, provides a plausible mechanism, although this interpretation might neglect substantial contributions, given that the full mutagenic potential of a DNA lesion is a consequence of not only its frequency and miscoding characteristics in the polymerase active site but also recognition of the modified base by DNA glycosylases, which seem to prefer other substrates over 5-OHC.[45−47] Our analysis of pre-steady-state kinetics of incorporation of dAMP opposite 5-substituted cytosine templates reveals that an electronegative moiety adjacent to C5 enhances formation of C·A mismatches by RB69 gp43. In conjunction with the crystal structures, which demonstrate a disposition for 5-OHC and 5-FC to unstack as template bases when there is no stabilizing guanine in the primer, this study restates the importance of base stacking for nucleotide selection by family B DNA polymerases, expanding the scope of this statement to include the templating base. Although dAMP is inserted opposite some lesions such as thymine glycol[23] or 8-oxoguanine[38,48−51] by WC or Hoogsteen base pairing, respectively, dAMP is also inserted opposite abasic sites because of enhanced stacking capabilities of the adenine base.[38,52−54] Therefore, it is not surprising that DNA synthesis opposite a disordered or unstacked template, like 5-OHC, could proceed similarly. As our knowledge of DNA lesions expands to include other oxidation products of DNA pairing with dAMP, such as the further oxidation products of guanine guanidinohydantoin and spiroiminodihydantoin,[33,55] it will be interesting to observe the extent to which, if any, transient abasic sites instruct misincorporation of adenine opposite other damaged DNA templates.

ASSOCIATED CONTENT

Supporting Information

Geometry of the DNA near the polymerase active site from the matched and mismatched structures compared to canonical DNA supports the similarities between the 5-OHC and 5-FC templates (Table S1). Evidence of the exonuclase complex is provided in the activity of wild-type gp43 on 5-OHC templates (Figure S1). This material is available free of charge via the Internet at http://pubs.acs.org.

AUTHOR INFORMATION

Corresponding Author

*S.D.: telephone, (802) 656-9531; fax, (802) 656-8749; e-mail, sdoublie@uvm.edu. S.S.W.: telephone, (802) 656-2164; fax, (802) 656-8749; e-mail, swallace@uvm.edu.

Funding

This work was supported by National Institutes of Health Grant CA52040 awarded by the National Cancer Institute. GM/CA CAT has been funded in whole or in part with Federal funds from the National Cancer Institute (Y1-CO-1020) and the National Institute of General Medical Sciences (Y1-GM-1104). Use of the Advance Photon Source was supported by the U.S. Department of Energy, Basic Energy Sciences, under Contract DE-AC02-06CH11357.

■ ACKNOWLEDGMENTS

Dr. Pierre Aller and Dr. Stéphanie Duclos were invaluable sources of assistance and conversation throughout our experiments. The data reduction and comparison strategies applied here were strongly influenced by Dr. Mark Rould. We acknowledge the GM/CA-CAT beamline staff at the APS for providing support and perpetually improving data collection tools.

■ ABBREVIATIONS

5-OHC, 5-hydroxycytosine; BER, base excision repair; 5-FC, 5-fluorocytosine; 5-MEC, 5-methylcytosine; UDG, uracil DNA glycosylase; KF, Klenow fragment; UG, uracil glycol; 5-OHU, 5-hydroxyuracil; WC, Watson−Crick; pol β, DNA polymerase β; 5′-TET, 5′-tetrachlorofluorescein; APS, Advanced Photon Source; pol ι, DNA polymerase ι; TDG, human thymine DNA glycosylase.

■ REFERENCES

(1) Richter, C., Park, J. W., and Ames, B. N. (1988) Normal oxidative damage to mitochondrial and nuclear DNA is extensive. *Proc. Natl. Acad. Sci. U.S.A. 85*, 6465−6467.

(2) Schaaper, R. M., and Dunn, R. L. (1991) Spontaneous mutation in the *Escherichia coli lacI* gene. *Genetics 129*, 317−326.

(3) Huang, M. E., Rio, A. G., Nicolas, A., and Kolodner, R. D. (2003) A genomewide screen in *Saccharomyces cerevisiae* for genes that suppress the accumulation of mutations. *Proc. Natl. Acad. Sci. U.S.A. 100*, 11529−11534.

(4) Nakken, S., Rodland, E. A., and Hovig, E. (2010) Impact of DNA physical properties on local sequence bias of human mutation. *Hum. Mutat. 31*, 1316−1325.

(5) Duncan, B. K., and Miller, J. H. (1980) Mutagenic deamination of cytosine residues in DNA. *Nature 287*, 560−561.

(6) Stivers, J. T., and Drohat, A. C. (2001) Uracil DNA glycosylase: Insights from a master catalyst. *Arch. Biochem. Biophys. 396*, 1−9.

(7) Cortazar, D., Kunz, C., Saito, Y., Steinacher, R., and Schar, P. (2007) The enigmatic thymine DNA glycosylase. *DNA Repair 6*, 489−504.

(8) Dizdaroglu, M., Laval, J., and Boiteux, S. (1993) Substrate specificity of the *Escherichia coli* endonuclease III: Excision of thymine- and cytosine-derived lesions in DNA produced by radiation-generated free radicals. *Biochemistry 32*, 12105−12111.

(9) Blaisdell, J. O., Hatahet, Z., and Wallace, S. S. (1999) A novel role for *Escherichia coli* endonuclease VIII in prevention of spontaneous G → T transversions. *J. Bacteriol. 181*, 6396−6402.

(10) Purmal, A. A., Kow, Y. W., and Wallace, S. S. (1994) Major oxidative products of cytosine, 5-hydroxycytosine and 5-hydroxyuracil, exhibit sequence context-dependent mispairing in vitro. *Nucleic Acids Res. 22*, 72−78.

(11) Feig, D. I., Sowers, L. C., and Loeb, L. A. (1994) Reverse chemical mutagenesis: Identification of the mutagenic lesions resulting from reactive oxygen species-mediated damage to DNA. *Proc. Natl. Acad. Sci. U.S.A. 91*, 6609−6613.

(12) Kreutzer, D. A., and Essigmann, J. M. (1998) Oxidized, deaminated cytosines are a source of C → T transitions in vivo. *Proc. Natl. Acad. Sci. U.S.A. 95*, 3578−3582.

(13) Tremblay, S., Douki, T., Cadet, J., and Wagner, J. R. (1999) 2′-Deoxycytidine glycols, a missing link in the free radical-mediated oxidation of DNA. *J. Biol. Chem. 274*, 20833−20838.

(14) Batra, V. K., Beard, W. A., Shock, D. D., Pedersen, L. C., and Wilson, S. H. (2008) Structures of DNA polymerase β with active-site mismatches suggest a transient abasic site intermediate during misincorporation. *Mol. Cell 30*, 315−324.

(15) Strauss, B. S. (2002) The "A" rule revisited: Polymerases as determinants of mutational specificity. *DNA Repair 1*, 125−135.

(16) Hogg, M., Wallace, S. S., and Doublié, S. (2004) Crystallographic snapshots of a replicative DNA polymerase encountering an abasic site. *EMBO J. 23*, 1483−1493.

(17) Zahn, K. E., Belrhali, H., Wallace, S. S., and Doublié, S. (2007) Caught bending the A-rule: Crystal structures of translesion DNA synthesis with a non-natural nucleotide. *Biochemistry 46*, 10551−10561.

(18) Franklin, M. C., Wang, J., and Steitz, T. A. (2001) Structure of the replicating complex of a pol α family DNA polymerase. *Cell 105*, 657−667.

(19) Hogg, M., Cooper, W., Reha-Krantz, L., and Wallace, S. S. (2006) Kinetics of error generation in homologous B-family DNA polymerases. *Nucleic Acids Res. 34*, 2528−2535.

(20) Hogg, M., Aller, P., Konigsberg, W., Wallace, S. S., and Doublié, S. (2007) Structural and biochemical investigation of the role in proofreading of a β hairpin loop found in the exonuclease domain of a replicative DNA polymerase of the B family. *J. Biol. Chem. 282*, 1432−1444.

(21) Otwinowski, Z., and Minor, W. (1997) Processing of X-ray diffraction data collected in oscillation mode. *Methods Enzymol. 276*, 307−325.

(22) Rould, M. A. (1997) Screening for heavy-atom derivatives and obtaining accurate isomorphous differences. *Methods Enzymol. 276*, 461−472.

(23) Aller, P., Rould, M. A., Hogg, M., Wallace, S. S., and Doublié, S. (2007) A structural rationale for stalling of a replicative DNA polymerase at the most common oxidative thymine lesion, thymine glycol. *Proc. Natl. Acad. Sci. U.S.A. 104*, 814−818.

(24) Brunger, A. T. (2007) Version 1.2 of the Crystallography and NMR system. *Nat. Protoc. 2*, 2728−2733.

(25) Emsley, P., and Cowtan, K. (2004) Coot: Model-building tools for molecular graphics. *Acta Crystallogr. D60*, 2126−2132.

(26) Murshudov, G. N., Skubak, P., Lebedev, A. A., Pannu, N. S., Steiner, R. A., Nicholls, R. A., Winn, M. D., Long, F., and Vagin, A. A. (2011) REFMAC5 for the refinement of macromolecular crystal structures. *Acta Crystallogr. D67*, 355−367.

(27) Howlin, B., Butler, S., Moss, D., Harris, G., and Driessen, H. (1993) TLSANL: TLS parameter-analysis program for segmented anisotropic refinement of macromolecular structures. *J. Appl. Crystallogr. 26*, 622−624.

(28) Vaisman, A., and Woodgate, R. (2001) Unique misinsertion specificity of poliota may decrease the mutagenic potential of deaminated cytosines. *EMBO J. 20*, 6520−6529.

(29) Wang, J., Sattar, A. K., Wang, C. C., Karam, J. D., Konigsberg, W. H., and Steitz, T. A. (1997) Crystal structure of a pol α family replication DNA polymerase from bacteriophage RB69. *Cell 89*, 1087−1099.

(30) Bebenek, A., Dressman, H. K., Carver, G. T., Ng, S., Petrov, V., Yang, G., Konigsberg, W. H., Karam, J. D., and Drake, J. W. (2001) Interacting fidelity defects in the replicative DNA polymerase of bacteriophage RB69. *J. Biol. Chem. 276*, 10387−10397.

(31) Johansson, E., and MacNeill, S. A. (2010) The eukaryotic replicative DNA polymerases take shape. *Trends Biochem. Sci. 35*, 339−347.

(32) McCulloch, S. D., and Kunkel, T. A. (2008) The fidelity of DNA synthesis by eukaryotic replicative and translesion synthesis polymerases. *Cell Res. 18*, 148−161.

(33) Aller, P., Ye, Y., Wallace, S. S., Burrows, C. J., and Doublié, S. (2010) Crystal structure of a replicative DNA polymerase bound to

the oxidized guanine lesion guanidinohydantoin. *Biochemistry 49*, 2502−2509.
(34) Ravishanker, G., Swaminathan, S., Beveridge, D. L., Lavery, R., and Sklenar, H. (1989) Conformational and helicoidal analysis of 30 PS of molecular dynamics on the d(CGCGAATTCGCG) double helix: "Curves", dials and windows. *J. Biomol. Struct. Dyn. 6*, 669−699.
(35) Yang, G., Wang, J., and Konigsberg, W. (2005) Base selectivity is impaired by mutants that perturb hydrogen bonding networks in the RB69 DNA polymerase active site. *Biochemistry 44*, 3338−3346.
(36) Beard, W. A., Shock, D. D., Batra, V. K., Pedersen, L. C., and Wilson, S. H. (2009) DNA polymerase β substrate specificity: Side chain modulation of the "A-rule". *J. Biol. Chem. 284*, 31680−31689.
(37) Obeid, S., Blatter, N., Kranaster, R., Schnur, A., Diederichs, K., Welte, W., and Marx, A. (2010) Replication through an abasic DNA lesion: Structural basis for adenine selectivity. *EMBO J. 29*, 1738−1747.
(38) Hogg, M., Rudnicki, J., Midkiff, J., Reha-Krantz, L., Doublié, S., and Wallace, S. S. (2010) Kinetics of mismatch formation opposite lesions by the replicative DNA polymerase from bacteriophage RB69. *Biochemistry 49*, 2317−2325.
(39) Suen, W., Spiro, T. G., Sowers, L. C., and Fresco, J. R. (1999) Identification by UV resonance Raman spectroscopy of an imino tautomer of 5-hydroxy-2′-deoxycytidine, a powerful base analog transition mutagen with a much higher unfavored tautomer frequency than that of the natural residue 2′-deoxycytidine. *Proc. Natl. Acad. Sci. U.S.A. 96*, 4500−4505.
(40) La Francois, C. J., Jang, Y. H., Cagin, T., Goddard, W. A. III, and Sowers, L. C. (2000) Conformation and proton configuration of pyrimidine deoxynucleoside oxidation damage products in water. *Chem. Res. Toxicol. 13*, 462−470.
(41) Bennett, M. T., Rodgers, M. T., Hebert, A. S., Ruslander, L. E., Eisele, L., and Drohat, A. C. (2006) Specificity of human thymine DNA glycosylase depends on N-glycosidic bond stability. *J. Am. Chem. Soc. 128*, 12510−12519.
(42) Patel, D. J., Kozlowski, S. A., Ikuta, S., and Itakura, K. (1984) Deoxyadenosine-deoxycytidine pairing in the d(C-G-C-G-A-A-T-T-C-A-C-G) duplex: Conformation and dynamics at and adjacent to the dA·dC mismatch site. *Biochemistry 23*, 3218−3226.
(43) Hunter, W. N., Brown, T., Anand, N. N., and Kennard, O. (1986) Structure of an adenine-cytosine base pair in DNA and its implications for mismatch repair. *Nature 320*, 552−555.
(44) Johnson, S. J., and Beese, L. S. (2004) Structures of mismatch replication errors observed in a DNA polymerase. *Cell 116*, 803−816.
(45) Wang, D., and Essigmann, J. M. (1997) Kinetics of oxidized cytosine repair by endonuclease III of *Escherichia coli*. *Biochemistry 36*, 8628−8633.
(46) D'Ham, C., Romieu, A., Jaquinod, M., Gasparutto, D., and Cadet, J. (1999) Excision of 5,6-dihydroxy-5,6-dihydrothymine, 5,6-dihydrothymine, and 5-hydroxycytosine from defined sequence oligonucleotides by *Escherichia coli* endonuclease III and Fpg proteins: Kinetic and mechanistic aspects. *Biochemistry 38*, 3335−3344.
(47) Tremblay, S., and Wagner, J. R. (2008) Dehydration, deamination and enzymatic repair of cytosine glycols from oxidized poly(dG-dC) and poly(dI-dC). *Nucleic Acids Res. 36*, 284−293.
(48) Hsu, G. W., Ober, M., Carell, T., and Beese, L. S. (2004) Error-prone replication of oxidatively damaged DNA by a high-fidelity DNA polymerase. *Nature 431*, 217−221.
(49) Brieba, L. G., Kokoska, R. J., Bebenek, K., Kunkel, T. A., and Ellenberger, T. (2005) A lysine residue in the fingers subdomain of T7 DNA polymerase modulates the miscoding potential of 8-oxo-7,8-dihydroguanosine. *Structure 13*, 1653−1659.
(50) Beckman, J., Wang, M., Blaha, G., Wang, J., and Konigsberg, W. H. (2010) Substitution of Ala for Tyr567 in RB69 DNA polymerase allows dAMP to be inserted opposite 7,8-dihydro-8-oxoguanine. *Biochemistry 49*, 4116−4125.
(51) Beard, W. A., Batra, V. K., and Wilson, S. H. (2010) DNA polymerase structure-based insight on the mutagenic properties of 8-oxoguanine. *Mutat. Res. 703*, 18−23.
(52) Freisinger, E., Grollman, A. P., Miller, H., and Kisker, C. (2004) Lesion (in)tolerance reveals insights into DNA replication fidelity. *EMBO J. 23*, 1494−1505.
(53) Zhang, X., Donnelly, A., Lee, I., and Berdis, A. J. (2006) Rational attempts to optimize non-natural nucleotides for selective incorporation opposite an abasic site. *Biochemistry 45*, 13293−13303.
(54) Zahn, K. E., Wallace, S. S., and Doublié, S. (2011) DNA polymerases provide a canon of strategies for translesion synthesis past oxidatively generated lesions. *Curr. Opin. Struct. Biol. 21*, 358−369.
(55) Burrows, C. J., Muller, J. G., Kornyushyna, O., Luo, W., Duarte, V., Leipold, M. D., and David, S. S. (2002) Structure and potential mutagenicity of new hydantoin products from guanosine and 8-oxo-7,8-dihydroguanine oxidation by transition metals. *Environ. Health Perspect. 110* (Suppl.5), 713−717.